Impact of horizontal resolution and model time step on European precipitation extremes in the OpenIFS 43r3 atmosphere model

Yingxue Liu[1,2], Joakim Kjellsson[1,2], Abhishek Savita[1] and Wonsun Park[3,4]

[1]GEOMAR Helmholtz Centre for Ocean Research Kiel, Kiel, Germany

[2]Faculty of Mathematics and Natural Sciences, Christian Albrechts University of Kiel, Kiel, Germany

[3]Center for Climate Physics, Institute for Basic Science (IBS), Busan, Republic of Korea

[4]Department of Integrated Climate System Science, Pusan National University, Busan, Republic of Korea

Correspondence to: Yingxue Liu (yiliu@geomar.de)

Abstract: Events of extreme precipitation pose a hazard to many parts of Europe but are typically not well represented in climate models. Here, we evaluate daily extreme precipitation over Europe during 1982–2019 in observations (GPCC), reanalysis (ERA5) and a set of atmosphere-only simulations at low- (100 km), medium- (50 km) and high- (25 km) horizontal resolution and also at different time steps (i.e., 60, 30 and 15 min) using low resolution (100 km) with identical vertical resolutions using OpenIFS (version 43r3). We find that both OpenIFS simulations and reanalysis underestimate the rates of extreme precipitation compared to observations. The biases are largest for the lowest resolution (100 km) and decrease with higher horizontal resolution (50 and 25 km) simulations in all seasons. The sensitivity to horizontal resolution is particularly high in mountain regions (such as the Alps, Scandinavia, Iberian Peninsula), likely linked to the sensitivity of vertical velocity to the representation of topography. The sensitivity of precipitation to model resolution increases dramatically with increasing percentiles, with modest biases in the 70th–80th percentile range and large biases above the 99th percentile range. We also find that precipitation above the 99th percentile mostly consists of large-scale precipitation (~80 %) in winter, while in summer it is mostly large-scale precipitation in Northern Europe (~70 %) and convective precipitation in Southern Europe (~70 %). Convective precipitation is more sensitive to model time step than to horizontal resolution. Large-scale precipitation increases significantly with both higher horizontal resolution and shorter model time step.

1. Introduction

38

39 Extreme precipitation events have severe impacts on our society and ecosystems. For example,
40 extreme precipitation caused a devastating flood in Germany in 2021, in which around 180
41 people died. The frequency and intensity of extreme precipitation are projected to increase over
42 most regions in the future (Intergovernmental Panel on Climate Change, 2023; Li et al., 2021;
43 Myhre et al., 2019). The increasing extreme precipitation poses a threat to society and must
44 thus be realistically simulated and projected accurately for future climates. However, the
45 climate models have large biases in simulating extreme precipitation events due to coarse
46 horizontal resolution grid and long model time step etc. (Alexander et al., 2019; Avila et al.,
47 2015; Sillmann et al., 2013). The model biases are also hard to evaluate as we lack long-term
48 observations. This study aims to understand the sensitivity of extreme precipitation to model
49 horizontal resolution and model time step.

50 Extreme precipitation events are usually underestimated in CMIP models (O'Gorman, 2015;
51 Sillmann et al., 2013). Some studies found the simulated extreme precipitation at higher
52 atmosphere horizontal resolutions is more realistic (Wehner et al., 2010, 2014). Jong et al.
53 (2023) found that the characteristics of extreme precipitation at 25 km resolution configurations
54 have smaller biases that at 50 and 100 km. While, Kopparla et al. (2013) found that the reduced
55 extreme precipitation biases at higher horizontal resolution do not hold for all regions (e.g.,
56 Australia).

57 Strandberg and Lind (2021) reported the effect of horizontal resolution on European extreme
58 precipitation is largest in regions with complex topography and in the summer season when
59 precipitation is mostly caused by convective processes using coupled models, in agreement
60 with Iles et al. (2020). However, Li et al. (2011) demonstrated that the impact of horizontal
61 resolution on global precipitation extremes is manifested mostly by its effects on large-scale
62 precipitation, which could be due to the improved large-scale circulation (Hack et al., 2006).
63 Other studies also found an increasing large-scale precipitation with higher resolution but the
64 convective precipitation is rather insensitive to resolution (Bacmeister et al., 2014; Jung et al.,
65 2012; Kopparla et al., 2013).

66

Both the individual physical parameterization in models and their coupling to the dynamics can benefit from a shorter time step (Jung et al., 2012). Mishra and Sahany (2011) found a more realistic simulation of the heavy precipitation in the tropics when the time step was shortened from 60 to 5 minutes at a coarse (~300 km) resolution in a short-period (12 months) configuration. Jung et al. (2012) also reported that the biases in tropical circulation are smaller at 15 minutes than 60 minutes in the IFS model, which is related to tropical precipitation although they did not work on the precipitation in their study. However, Roberts et al. (2018) found a minimal impact on model biases when shortening the time step from 20 to 15 minutes at 25 km in the IFS model. They either did not investigate the multi-year precipitation extremes, or did not explore the extremes in IFS model.

The sensitivity of climate model performance to horizontal resolution and model time step exists in many models, but the level of sensitivity varies considerably between models and studied regions. Most of the global atmosphere-models do not explicitly resolve all the physical processes and must therefore employ parametrizations to represent those unresolved processes (spatially or temporally), which shows a weakness in the models. A recent study by Savita et al. (2024) explored the sensitivity of global mean precipitation to the horizontal resolution and model time step in atmosphere-only simulations with OpenIFS. However, the extreme precipitation's sensitivity to horizontal resolution and time step was not investigated. In this study, we investigated the impact of horizontal resolutions (~100 km, ~50 km, and ~25 km) and model time steps (60 minutes, 30 minutes, and 15 minutes) on daily extreme precipitation using OpenIFS simulations and compare them with observation. We also studied the convective and large-scale precipitation in all simulations. Precipitation extremes sensitivity to model time step is the first time explored in this work using 100 km in OpenIFS atmosphere model. Besides the extremes, we also explored multi-percentile precipitation's sensitivity to horizontal resolution and time step. This paper is structured as follows: section 2 describes the data and methodology, and section 3 discusses the results. The conclusion and discussion can be found in section 4.

2. Data and Methods

2.1 Model, observation, and reanalysis data

The OpenIFS is derived from the Integrated Forecasting System at the European Centre for Medium-range Weather Forecasting (ECMWF-IFS) cycle 43 release 3 (43r3) (ECMWF, 2017). We use the same AMIP simulations that were used in Savita et al. (2024) which cover the period 1979-2014 and are extended to 2019 using sea-surface temperature (SST) from ERA5 and the Shared Socioeconomic Pathway 5 (SSP5-8.5) scenario from CMIP6. OpenIFS simulations use 91 vertical levels (L91) and the different horizontal resolutions: low resolution (Tco95, ~100 km), medium resolution (Tco199, ~50 km), and high resolution (Tco399, ~25 km). For the low resolution, additional sensitivity experiments use different model time steps i.e., 60, 30, and 15 minutes and we refer to these experiments as LR60m, LR30m, and LR, respectively. For medium and high resolution, the same model time step is used (i.e., 15 minutes), of which experiments refer to as MR and HR, respectively. While the OpenIFS uses a reduced octahedral grid (Malardel et al., 2016), the final output used in this study has been interpolated to a regular grid using the second-order conservative method (Kritsikis et al., 2017) by XIOS output server. The LR, LR30m and LR60m output were interpolated to a global 0.9° regular grid while the MR and HR output were interpolated to a global 0.45° regular grid, i.e., we are not investigating extreme precipitation in high resolution simulations in their native reduced octahedral grid, which will be investigated in future study. The simulations used here were used by Savita et al. (2024) who found improvements in the surface zonal wind, Rossby wave amplitude and phase speed, weather regime patterns, and surface-air temperature when shortening a model time step from 60 minutes to 30 and 15 minutes in low resolution or increasing the horizontal resolution from 100 km to 50 and 25 km. However, Savita et al. (2024) did not find such improvement in the mean precipitation bias by increasing horizontal resolution or shortening the model time step.

To validate OpenIFS simulations, we use the gridded daily precipitation observational data from Global Precipitation Climatology Centre (GPCC) with resolution of 1° × 1° for the period 1982−2019 (Ziese et al., 2022) as well as the reanalysis data from the ECMWF Reanalysis v5 (ERA5) for 1979−2019 (Hersbach et al., 2023). ERA5 is based on the IFS Cy41r2, with 31 km horizontal resolution and 137 levels (Hersbach et al., 2020). We analyzed total, large-scale, and convective precipitation in this study. The total precipitation (convective plus large-scale

133   precipitation) in the IFS is the accumulated precipitation, comprising of rain and snow, that

134   falls to the Earth's surface, and it is not assimilated in the IFS. The convective precipitation is

135   generated by the convection scheme in the IFS, which represents convection at spatial scales

136   smaller than the grid box. The convection scheme follows Sundqvist (1978), which is also used

137   in the OpenIFS. The large-scale precipitation is generated by the cloud scheme (Khairoutdinov

138   and Kogan, 2000), which represents the formation and dissipation of clouds and large-scale

139   precipitation due to changes in atmospheric quantities (such as pressure, temperature, and

140   moisture) predicted directly by the IFS at spatial scales of the grid box or larger. The

141   autoconversion/accretion parameterization is a non-linear function of the mass of both liquid

142   cloud and rainwater. The calculation follows Khairoutdinov and Kogan (2000) which is derived

143   from large eddy simulation studies of drizzling stratocumulus clouds, and this scheme is also

144   used in OpenIFS. Several studies have evaluated the performance of ERA5 and found that the

145   total precipitation in ERA5 is performing well over the US (Tarek et al., 2020; Xu et al., 2019).

146   For global precipitation, the mean absolute difference over 50° S–50° N between ERA5 and

147   TRMM/3B43 is 0.58 mm/d; the global-mean correlation with GPCP data is 0.77, which is

148   better compared to ERA-Interim (0.63 mm/d and 0.67) (Hersbach et al., 2020). ERA5 also

149   performs well in polar regions in representing wind, temperature and humidity (Graham et al.,

150   2019; Tetzner et al., 2019; Wang et al., 2019).

151   Here we analyze daily ERA5 and the OpenIFS data over Europe (30° N–72° N, 10° W–40° E)

152   for the period of 1982–2019 to be consistent with the GPCC dataset. For comparison, the ERA5,

153   GPCC, MR, and HR data are remapped to LR (~0.9375° × 0.9375°) using the second-order

154   conservative remapping method, which is consistent with the XIOS server used. The second-

155   order conservative method includes the gradient across the source cell, which is not included

156   in the first-order conservative method. Therefore, it gives a smoother, more accurate

157   representation of the source field (Jones, 1998).

158
159   **2.2 Methods**

160   **Calculation of qth percentile value**

161   We calculated different percentile values using total precipitation from GPCC, ERA5, and

162   OpenIFS simulations. When we calculated the qth percentile value, the normalized ranking

163   usually did not match the location of the qth percentile exactly, which means the qth lies between

164   two indices. Therefore, we determined the location first, then computed the qth value by

interpolating between the two nearest values based on the location. Here we used the formula below to find the location:

$$j = q*(n-1) \tag{1}$$

n is the length of the sample, q is the desired percentile, j is the location which is the distance from the first value X_1 (X_m are the sorted sample values, m=1, 2, …, n). Then we took i as the nearest (lower) integer of j to get the qth value P(q) by interpolating.

$$P(q) = X_i + (X_{i+1} - X_i) * (j-i) \tag{2}$$

There are other methods to determine the location of qth percentile (Hyndman and Fan, 1996), but here we use the 'linear' one.

The large-scale precipitation contribution to extreme precipitation

To calculate the contribution of large-scale precipitation to total precipitation for a percentile range, at each grid point we accumulated the large-scale precipitation on all days when the total precipitation is in that percentile range, then divided it by the accumulated total precipitation on those days to get the fraction of large-scale precipitation.

Calculation of RMSE values

We used the root-mean-square error (RMSE) referenced to GPCC that measures the performance of ERA5 and OpenIFS simulations:

$$RMSE = \sqrt{\frac{\sum_{i=1}^{n}(x_{mi}-x_{oi})^2}{n}} \tag{3}$$

x_{mi} is the value at i grid point for ERA5 or OpenIFS simulations, x_{oi} is the value for GPCC, n is the number of land grid points over Europe. Using equation (3), we calculated the RMSE values for different percentile ranges. Smaller RMSE values mean the biases between OpenIFS (or ERA5) and GPCC are smaller i.e., the model simulations and ERA5 are performing better. The relative RMSE (RRMSE) is calculated by dividing the RMSE by GPCC precipitation at corresponding percentile range.

Confidence intervals

We calculated the 2.5 to 97.5[th] confidence intervals (CI) for the RMSE for each percentile with a bootstrap method. For example, to calculate the CI for the RMSE of HR (referenced to GPCC observation), we randomly chose n grid cell pairs from GPCC and HR over European land, then calculated their RMSE (n is the number of total land grid points over Europe). This process was repeated for *2000* times. We took the 2.5[th] and 97.5[th] percentiles of the distribution of the

198 2000 RMSEs as the 95 % CI. If the CI for different simulations do not overlap then we refer

199 that they are significantly different.

200

3. Results

201

202

3.1 Extreme precipitation over Europe

203

204

205 We show the time series of 99th percentile precipitation calculated from all grid points and all

206 days in each year over the period 1982−2019 from GPCC, ERA5, and OpenIFS simulations

207 over Europe (Fig. 1). The ERA5 simulates an inter-annual variability of the 99th percentile

208 precipitation similar to that in GPCC. For example, the peak in 2010 and the low in 1994 are

209 well reproduced in the ERA5. ERA5 is a reanalysis product that assimilates observation of

210 precipitation, therefore, we expect it to do a better job of reproducing dry (1994) and wet (2010)

211 years than OpenIFS simulations that do not reproduce the same inter-annual variability as in

212 GPCC or ERA5. However, LR and HR do reproduce the 95 % significant positive trend

213 observed in GPCC (0.03 mm/d/y, not shown), which are ~0.02 mm/d/y for both LR and HR,

214 and it is not significant for MR. We note that the OpenIFS simulations use observed SST and

215 sea-ice concentrations as boundary conditions, but ozone is taken from a photochemical

216 equilibrium (Cariolle and Teyssèdre, 2007) and aerosol concentrations are taken from

217 Copernicus Atmosphere Monitoring Service (CAMS) monthly climatology. Therefore, we do

218 not expect LR, MR and HR to reproduce trends driven by ozone or aerosols forcing. We also

219 find that both ERA5 and OpenIFS simulations have relatively lower 99th percentile

220 precipitation rates compared to GPCC (Fig. 1). The RMSE for ERA5 (0.36 mm/d) is lower

221 than for OpenIFS simulations which is largest for LR (2.03 mm/d) and decreases with higher

222 horizontal resolution (i.e., 1.13 mm/d for MR and 0.69 mm/d for HR). Note that Fig. 1 does

223 not contain any spatial information and that a mismatch between model data and observations

224 can be due to the 99th percentile occurring in different regions and/or with different magnitudes.

225 The RMSE analysis suggests that ERA5 and HR are close to GPCC and LR is far from GPCC.

226

227 Figure 2a−e shows the spatial distribution of the 99th percentile precipitation over Europe for

228 all days in each season for all years in GPCC, ERA5, and OpenIFS simulations, respectively.

229 In general, the extreme precipitation is very low (~ 2 mm/d) in Northern Africa, which is to be

230 expected since the mean precipitation is only 0.5 mm/d in those regions (Fig. S1). The extreme

231 precipitation exceeds 30 mm/d over mountain areas (e.g., Scandinavian mountains, Alps, and

232 Iberian Peninsula) and the north coast of the Mediterranean but is otherwise lower (~15 mm/d).

233   The spatial distribution of extreme precipitation matches that of the mean precipitation pattern
234   (Fig. S1). The high 99th percentile precipitation near mountains is likely due to the forced ascent
235   of westerly (Scandinavia, Iberian Peninsula, British Isles) and southerly (Alps) winds. The high
236   99th percentile precipitation in the north of the Mediterranean is likely because of warm and
237   moist southerly winds from the Mediterranean Sea. The ERA5 and OpenIFS simulations
238   overall reproduce the spatial distribution of the 99th percentile precipitation from GPCC.
239   However, the magnitudes are different, particularly over the Scandinavian mountains, the Alps,
240   and central Europe near 50° N (Fig. 2a–e). Figure 2f–i show the regional biases for the 99th
241   percentile precipitation referenced to GPCC. LR mostly underestimates the 99th percentile
242   precipitation in mountainous areas and deserts by more than 25 % (Fig. 2g) and the biases are
243   reduced when horizontal resolution is increased in MR and HR (Fig. 2h–i). We also notice that
244   LR underestimates the 99th percentile precipitation south of the Alps but overestimates it to the
245   north (Fig. 2 (g)), whereas this bias is negligible in higher-resolution simulations (Fig. 2h–i).
246   This is due to the lower and gentler Alps region simulated in LR (Fig. S2), where the moist
247   southerly winds do not ascend high enough, therefore there is less precipitation formed on the
248   southern side and more moisture is advected over the mountain. The moist air descends more
249   slowly over gentler leeward side in LR than MR (HR), thus the leeward region may get more
250   precipitation. The reduced biases near mountain regions in the higher-resolution simulations
251   are likely because higher resolution has a better representation of topography and vertical
252   velocity. A cross section of the topography and annual-mean vertical velocity at 850 hPa and
253   62° N (Fig. S3a&b) highlight that the higher-resolution simulations resolve steeper topography,
254   which leads to more ascent and thus more precipitation.
255
256   The 99th percentile precipitation over the Alps is more realistic with higher horizontal
257   resolution compared to lower resolution. However, all simulations as well as ERA5 exhibit a
258   negative bias over northeast Italy and west Slovenia (Fig. 2f–i). By analyzing the EOBS data,
259   we find a similar negative bias as in GPCC, but a positive bias in GPCP (Fig. S4d-k). We notice
260   that the extreme precipitation over the Alps (including Slovenia) in GPCP is lower than GPCC
261   and EOBS (Fig. S4a-c), which is likely due to the different data sources and grid methods in
262   different observation datasets (e.g., GPCC and EOBS are gauge-based gridded data on the land,
263   but GPCP data combines microwave and infrared measurements, satellites and rain gauges).
264   We do not know which observation dataset is more realistic, therefore, the cause of the negative
265   bias near Slovenia could be a bias in GPCC or a persistent model bias in the ECMWF-IFS on

8

which both ERA5 and OpenIFS are based. In general, ERA5 has a lower RMSE (2.6 mm/d) for extreme total precipitation than OpenIFS simulations, i.e., ERA5 has overall lower biases than LR (4.0 mm/d) and is similar to MR (3.0 mm/d) and HR (2.9 mm/d).

We next calculate the trend for the annual 99th percentile precipitation over Europe (Fig. 3 & 4) and find that the 99th percentile precipitation has a large positive trend in central Europe and a negative trend to the north of the Alps in GPCC (Fig. 3a). The ERA5 reproduces the pattern of the trend found in GPCC but is not significant. However, OpenIFS simulations do not have consistent patterns with GPCC (Fig. 3d–f, Fig. 4d–f), with only LR30m reproducing the large positive trend in central Europe (Fig. 4d). Overall, the trend is largely underestimated over central Europe but overestimated over northern Europe in OpenIFS simulations. We have not found any consistent improvement across the horizontal resolution and model time step.

In addition to the 99th percentile precipitation and the trend, we calculate annual total precipitation in different percentile ranges, such as 70th–80th, 80th–90th, 90th–95th, 95th–99th, 99th–99.5th, 99.5th–99.9th and larger than 99.9th (i.e., >99.9th) percentile. The RMSEs for ERA5 and OpenIFS simulations referenced to GPCC in each range are shown in Fig. 5. The RMSEs increase exponentially with increasing percentiles, from less than 1 mm/d at the 70th–80th percentile range to ~8 mm/d above the 99.9th percentile range. The largest RMSE is found for LR60m above the 99.9th percentile range which is around 12 mm/d [CI: 11.3–12.8 mm/d]. We also find that the RMSEs decrease with finer horizontal resolution for all percentile ranges. The CI of the RMSEs from LR do not overlap with those from higher horizontal resolutions for any percentile range, i.e., the biases from LR are significantly different from that at higher resolutions and thus clearly sensitive to the horizontal resolution. Notably, the RMSE differences between LR simulation and the higher-resolution simulations as well as ERA5 are larger at higher percentile ranges (>95th) than those at lower percentile ranges (<95th). This suggests that the extreme precipitation is more sensitive to horizontal resolution than precipitation at lower percentile ranges (<95th). ERA5 has the smallest RMSE of all datasets above the 95th percentile ranges, i.e., ERA5 has a better representation of the extreme precipitation than our OpenIFS simulations (Fig. 5).

The RMSEs for LR60m, LR30m, and LR are smaller when the model time step is shorter. However, the CI of RMSE overlaps at all percentile ranges, i.e., the sensitivity of precipitation

9

to the model time step is not statistically significant in the low-resolution configurations. While the model time step may influence precipitation, especially convective precipitation, errors from poorly resolved topography probably have a large impact on the RMSE, which would explain the lack of sensitivity to the model time step.

The above analysis is based on the RMSE values, which measure the absolute magnitude of biases. The exponential increase in RMSE with higher percentiles is due to the corresponding exponential increase in precipitation amounts across those percentiles. The relative biases are further explored by calculating the relative RMSE (RRMSE) (Fig. S5). For the precipitation above 90th percentile (> 6 mm/d), RRMSEs are larger at higher percentiles (>99.9th percentile) than lower percentiles (90-95th percentile). A larger sensitivity to horizontal resolution at higher percentiles can be also seen, since the RRMSE differences between LR and MR (HR) slightly increase from 5.5% at 90-95th to 6.9% above 99.9th percentile. The above RRMSEs' results are qualitatively consistent with the larger RMSE and sensitivity to horizontal resolution at higher percentiles shown in Fig. 5, but quantitatively RRMSE shows smaller variations across percentiles than RMSE does. However, the RRMSE at 70-90th percentile ranges show comparable magnitude and sensitivity to those above 99th percentile, which is related to the very low precipitation amounts at these percentiles (1.9 mm/d for 70-80th and 3.6 mm/d for 80-90th percentile range).

3.2 Relative roles of convective and large-scale precipitation

Total precipitation is the sum of convective and large-scale precipitation. Convective precipitation is related to unresolved convective motions. It comes from the physical processes whose scales are smaller than the resolution of the model, therefore need to be parametrized. On the other hand, large-scale precipitation is related to large-scale processes larger than the model resolution, that can be resolved. When moving to higher horizontal resolutions, large-scale precipitation is likely to increase, and the ratio between convective and large-scale precipitation may change. In this section we split the extreme precipitation into convective and large-scale precipitation to see their sensitivities to horizontal resolution and model time step. The extreme precipitation is nearly 100 % large-scale precipitation over northern Europe, more than 90 % over central Europe, and more than 70 % over western and southern Europe in DJF (Fig. 6e–h). However, in JJA the extreme precipitation is mostly large-scale precipitation over northern Europe (>70 %) and convective precipitation in the Mediterranean region (>70 %)

(Fig. 6a–d). Due to the seasonal dependent large-scale precipitation contribution to extreme total precipitation, we discuss convective and large-scale precipitation's sensitivities to horizontal resolution and time step in JJA and DJF separately. The ratios between convective and large-scale precipitation are also discussed here. Considering the ratios over parts of Mediterranean region are very large, which influence the results a lot, we remove that region and only include the region north than 40°N (i.e., 40° N–72° N, 10° W–40° E) in this section.

During the extreme precipitation days, Europe has more convective precipitation in JJA (~10 mm/d) than in DJF (~3.7 mm/d), and their distributions do not change much across horizontal resolution (Fig. 7a & b). While, from the significant test (Table 2a), we found JJA convective precipitation only increases significantly moving from MR to HR, and DJF convective precipitation significantly increases from LR to MR (HR). However, convective precipitation's distributions vary noticeably across model time steps, as shown in Fig. 7 c & d. As the model time step reduces, the distributions of JJA convective precipitation move to the left, thus less convective precipitation are simulated in shorter time step simulations. DJF has similar results as in JJA. The changes are significant (Table 2a), that is, convective precipitation in OpenIFS is sensitive to model time step.

The distributions of large-scale precipitation in MR and HR (Fig. 7e) shift to the right compared to LR in JJA, and MR and HR have significantly more large-scale precipitation (13.2 mm/d) than LR (11.4 mm/d). In DJF, the distribution peak of LR, MR and HR are similar (Fig. 7f), but MR and HR have bigger tails than LR. Thus, MR and HR have more large-scale precipitation than LR. The increase of large-scale precipitation is likely due to the better simulated topography at higher horizontal resolution, where more large-scale precipitation is resolved. The changes of large-scale precipitation in both JJA and DJF from LR to MR are significant, but not from MR to HR (Table 2b). That means, the large-scale precipitation is sensitive when horizontal resolution is increased from LR to MR, but not from MR to HR. Large-scale precipitation also significantly increases when the model time step is shorten from 60 min to 30 min, and also from 30 min to 15 min in both JJA (Fig. 7g) and DJF (Fig. 7h), that is large-scale precipitation is also sensitive to the model time step.

We further analyse the distribution of ratio between convective and large-scale precipitation in JJA and DJF, shown in Fig. 8. For different resolutions, the ratio distributions from MR and HR are narrower and slightly shift to the left compared to LR in JJA (Fig. 8a), which means

367   MR and HR have smaller mean ratios (1.5) than LR (~1.25). That is due to the large-scale
368   precipitation increasing by 16% with finer horizontal resolution, whereas convective
369   precipitation only increases by 6%. However, the ratio between convective and large-scale
370   precipitation do not vary significantly with higher horizontal resolutions in DJF (Fig. 8b).
371   When moving to shorter model time step, the ratios significantly decrease in JJA (from 2 to
372   1.5) and DJF (Fig. 8c-d, Table 2c). It is related to the significant decreasing convective and
373   increasing large-scale precipitation with shorter model time step.

374

375   In summary, during extreme precipitation days, large-scale precipitation increases with higher
376   horizontal resolution and shorter model time step, however, convective precipitation increases
377   with higher horizontal resolution and decrease with shorter model time step. Convective
378   precipitation is more sensitive to model time steps than to horizontal resolutions, while large-
379   scale precipitation is sensitive to both. Therefore, the extreme precipitation sensitivity to
380   horizontal resolution is mostly from large-scale precipitation.

381

382   We also analyse the mean state convective and large-scale precipitation's sensitivity to
383   horizontal resolution and model time step (Fig. S6 & S7). Convective precipitation decreases
384   and large-scale precipitation increases with higher horizontal resolution and shorter model time
385   step, therefore their ratio decreases. Their sensitivities to resolutions and time steps are less
386   significant in mean state than in extreme state, especially for mean convective precipitation,
387   which is only significantly sensitive when shortening model time step from 30 min to 15 min.
388   The changes of mean convective precipitation with horizontal resolution are opposite with the
389   extreme one (Fig. S6a & b, Fig. 7a & b), but these changes for both extreme and mean states
390   are very little, and convective precipitation is more sensitive to model time steps in both states
391   (Fig. S6c & d, Fig. 7c & d).

392

393   **4. Discussion and Conclusion**
394   We have investigated the sensitivity of extreme precipitation across different horizontal
395   resolutions and model time steps in atmosphere-only experiments with the OpenIFS.
396   Comparing extreme precipitation (defined as total daily precipitation at the 99th percentile)
397   from OpenIFS simulations, reanalysis (ERA5), and observation (GPCC), we find that MR and
398   HR mostly better represent the precipitation extremes compared to LR. We also found a more
399   significant sensitivity to the horizontal resolution for the precipitation above the 95th percentile
400   and less sensitivity for lower percentile ranges (<95th) (Fig. 5). These OpenIFS-based results

401 are similar to Kopparla et al. (2013), who found that the bias of extreme precipitation in the
402 high-resolution simulation (25 km) is reduced compared to the lower-resolution simulations
403 (100 km and 200 km) over Europe in their atmospheric model, but not for precipitation at lower
404 percentiles (i.e., <95th). However, the sensitivity to the horizontal resolution found by Kopparla
405 et al. (2013) was not significant over Europe which is rather different from our results as we
406 have found a significant difference across the horizontal resolutions. In contrast to the extreme
407 precipitation, the bias for global mean precipitation is not decreasing much with higher
408 horizontal resolution in OpenIFS. Similar results are also found in other AGCMs (e.g.,
409 ECHAM6, OpenIFS, HadGEM1 and HadGEM3) (Hertwig et al., 2015; Savita et al., 2024;
410 Schiemann et al., 2014; Demory et al., 2020;). However, Delworth et al. (2012) found an
411 improvement in the global mean precipitation with higher horizontal resolution in a coupled
412 model (GFDL).
413
414 The improvements due to higher horizontal resolution for the extreme precipitation are mostly
415 over the mountain areas, consistent with previous studies which found the effect of horizontal
416 resolution being largest in areas with complex topography over Europe and also other regions
417 for mean and extreme precipitation (Demory et al., 2020; Iles et al., 2020; Monerie et al., 2020;
418 Prein et al., 2013; Torma et al., 2015). The sensitivity to the horizontal resolution comes from
419 the large-scale precipitation, which is likely because of the better-resolved topography.
420 However, the convective precipitation is more sensitive to the model time step than it is to the
421 horizontal resolution.
422
423 In our results, larger improvements are obtained when the horizontal resolution is increased
424 from LR to MR, but relatively smaller improvements from MR to HR. This diminishing return
425 is also found by Roberts et al. (2018) from ~50 km to ~25 km in ECMWF-IFS, but for
426 climatological surface biases. The simulation of extratropical cyclones, tropospheric
427 circulation and tropical mean precipitation in ECMWF-IFS also have smaller improvements
428 from 39 km to 16 km than that from 126 km to 39 km (Jung et al., 2012). However, the tropical
429 cyclone intensity and intense storm structure, which often cause extreme precipitation in tropics
430 (Gori et al., 2022; Zhu and Quiring, 2022) are adequately simulated at 16 km, but not at 126
431 and 39 km resolutions in ECMWF-IFS (Manganello et al., 2012). Therefore, the diminishing
432 return in this study is valid for European extreme precipitation, but may not for tropical extreme
433 precipitation.
434

435   Since the analysis of horizontal resolution's impact is based on regridded data, may therefore

436   be influenced by the regridding process. The native resolution of our model output is 192×384

437   for LR, 400×800 for MR and 800×1600 for HR, however, only 400×800 for HR output is saved

438   due to computational cost.   Similar to the result of regridded data (Fig. 1), extreme

439   precipitation on their native resolution is underestimated in OpenIFS compared to GPCC, and

440   the biases decrease with higher horizontal resolution (Fig. 9). Extreme precipitation on native

441   resolutions also has similar spatial distribution with that on regridded resolution (Fig. 10, Fig.

442   2), such as more extreme precipitation in mountain areas. However, the extreme precipitation

443   is larger (13% for GPCC, 7% for MR and 12% HR) on native resolution than on regridded

444   resolution, because some extreme precipitation is smoothed when regridding to 0.9×0.9

445   degree. The RMSEs of extreme precipitation against GPCC are also larger on native resolution

446   (Fig. 9) than on regridded resolution (Fig. 1), which holds across different percentiles (Fig. S8).

447   Moreover, the sensitivity of extreme precipitation to horizontal resolution is also greater on

448   native resolution (Fig. S8).   Convective and large-scale precipitation during extreme

449   precipitation days increase with higher horizontal resolution (Fig. 11 a-d), consistent with

450   regridded results. The convective-to-large-scale precipitation ratio significantly decreases from

451   LR to MR in JJA (Fig. 11e), which is also consistent with regridded results. However, the ratio

452   increases from MR to HR in JJA on native resolution, differing from regridded analysis, likely

453   due to the dramatic increasing convective precipitation from MR to HR in JJA. Overall,

454   regridding the model dataset does not change the conclusion qualitatively in this study but

455   causes quantitative differences.

456

457   Moreover, the choice of observation dataset is a key factor for assessing the impact of the

458   horizontal resolution and model time step on extreme precipitation. Most observation

459   precipitation data are from one of the three categories, gauge-based products, satellite products,

460   and merged satellite-gauge products. Since the satellite products are constructed with satellite

461   microwave and/ or infrared measurements, with/ without gauged-adjusted estimates,

462   differences exist between these products. Besides, the gauge-based products are highly

463   dependent on the choice of stations and interpolation schemes. It is hard to say which product

464   is closer to reality, as different regions may have different observation datasets that suit best

465   for the analysis. In particular, we note that not all products are suitable for extreme analysis.

466   For example, GPCP's main scope is to construct a reliable climate data record and has been

467   developed with a priority of ensuring the long-term stability of data (Adler et al., 2017).

468   Masunaga et al. (2019) found that the frequency of GPCP daily precipitation quickly drops

469 below all other datasets once the precipitation exceeds 30 mm/d. Also, the time series of GPCP

470 extreme precipitation over the ocean exhibits a jump to lower 99th percentiles in late 2008/early

471 2009 which is not present in all other datasets, coinciding with the change in utilization of

472 SSM/I and SSMIS. The lower 99th precipitation suggests that the GPCP dataset might not be

473 applied to extreme analysis (Masunaga et al., 2019). Therefore, we only use GPCC observation

474 data as the reference to explore the model performance. In Fig. 2f–i the 99th percentile

475 precipitation is largely underestimated in the eastern Alp region by ERA5 and all model

476 simulations. The biases are insensitive to horizontal resolution. It is likely a persistent model

477 bias in the ECMWF-IFS or a bias in GPCC. Comparing model output to multiple observational

478 precipitation products instead of relying on a single one may be a good way to reduce these

479 biases. Multiple observational products can be taken as an ensemble, which provide a spread

480 of observational estimates and allow insights into whether and which model configurations sit

481 within this observational spread.

482

483 **Code and data variability**

484 The OpenIFS model requires a software license agreement with ECMWF to use it, and

485 OpenIFS's license is easily given free of charge to any academic or research institute. The

486 details of OpenIFS are available at

487 https://confluence.ecmwf.int/display/OIFS/About+OpenIFS (ECMWF, 2018). We used the

488 same simulation that used in Savita et al. (2024) and therefore do not provide the data needed

489 to reproduce the simulations here. All data (runscripts, input data etc) needed to reproduce the

490 simulations can be found in Savita et al. (2024) in code and data variability section. The jupyter

491 notebook scripts used in this study to produce the plots can be found at

492 https://doi.org/10.5281/zenodo.15497274. The raw model output is available from the authors

493 upon reasonable request. The observation and reanalysis datasets used in this study can be

494 downloaded from GPCC (https://opendata.dwd.de/climate_environment/GPCC/html/fulldata-

495 daily_v2022_doi_download.html, Ziese et al., 2022) and ERA5

496 (https://cds.climate.copernicus.eu/cdsapp#!/dataset/reanalysis-era5-single-levels?tab=form,

497 Hersbach et al., 2023).

498

499 **Authors contributions.** AS and JK conducted all the OpenIFS simulations. YL did the

500 analysis and writing with substantial contribution from JK, AS and WP.

501

535

References

Adler, R. F., Gu, G., Sapiano, M., Wang, J. J., and Huffman, G. J.: Global Precipitation: Means, Variations and Trends During the Satellite Era (1979–2014), https://doi.org/10.1007/s10712-017-9416-4, 1 July 2017.

Alexander, L. V., Fowler, H. J., Bador, M., Behrangi, A., Donat, M. G., Dunn, R., Funk, C., Goldie, J., Lewis, E., Rogé, M., Seneviratne, S. I., and Venugopal, V.: On the use of indices to study extreme precipitation on sub-daily and daily timescales, Environmental Research Letters, 14, https://doi.org/10.1088/1748-9326/ab51b6, 2019.

Avila, F. B., Dong, S., Menang, K. P., Rajczak, J., Renom, M., Donat, M. G., and Alexander, L. V.: Systematic investigation of gridding-related scaling effects on annual statistics of daily temperature and precipitation maxima: A case study for south-east Australia, Weather Clim Extrem, 9, 6–16, https://doi.org/10.1016/j.wace.2015.06.003, 2015.

Bacmeister, J. T., Wehner, M. F., Neale, R. B., Gettelman, A., Hannay, C., Lauritzen, P. H., Caron, J. M., and Truesdale, J. E.: Exploratory high-resolution climate simulations using the community atmosphere model (CAM), J Clim, 27, 3073–3099, https://doi.org/10.1175/JCLI-D-13-00387.1, 2014.

Bell, B., Hersbach, H., Simmons, A., Berrisford, P., Dahlgren, P., Horányi, A., Muñoz-Sabater, J., Nicolas, J., Radu, R., Schepers, D., Soci, C., Villaume, S., Bidlot, J. R., Haimberger, L., Woollen, J., Buontempo, C., and Thépaut, J. N.: The ERA5 global reanalysis: Preliminary extension to 1950, Quarterly Journal of the Royal Meteorological Society, 147, 4186–4227, https://doi.org/10.1002/qj.4174, 2021.

Cariolle, D. and Teyssèdre, H.: Atmospheric Chemistry and Physics A revised linear ozone photochemistry parameterization for use in transport and general circulation models: multi-annual simulations, Atmos. Chem. Phys, 2183–2196 pp., 2007.

Delworth, T. L., Rosati, A., Anderson, W., Adcroft, A. J., Balaji, V., Benson, R., Dixon, K., Griffies, S. M., Lee, H. C., Pacanowski, R. C., Vecchi, G. A., Wittenberg, A. T., Zeng, F., and Zhang, R.: Simulated climate and climate change in the GFDL CM2.5 high-resolution coupled climate model, J Clim, 25, 2755–2781, https://doi.org/10.1175/JCLI-D-11-00316.1, 2012.

Demory, M. E., Berthou, S., Fernández, J., Sørland, S. L., Brogli, R., Roberts, M. J., Beyerle, U., Seddon, J., Haarsma, R., Schär, C., Buonomo, E., Christensen, O. B., Ciarlo, J. M., Fealy, R., Nikulin, G., Peano, D., Putrasahan, D., Roberts, C. D., Senan, R., Steger, C., Teichmann, C., and Vautard, R.: European daily precipitation according to EURO-CORDEX regional climate models (RCMs) and high-resolution global climate models (GCMs) from the High-Resolution Model Intercomparison Project (HighResMIP), Geosci Model Dev, 13, 5485–5506, https://doi.org/10.5194/gmd-13-5485-2020, 2020.

ECMWF: IFS Documentation CY43R3 - Part IV: Physical processes, https://doi.org/10.21957/efyk72kl, 2017.

Gori, A., Lin, N., Xi, D., and Emanuel, K.: Tropical cyclone climatology change greatly exacerbates US extreme rainfall–surge hazard, Nat Clim Chang, 12, 171–178, https://doi.org/10.1038/s41558-021-01272-7, 2022.

Graham, R. M., Hudson, S. R., and Maturilli, M.: Improved Performance of ERA5 in Arctic Gateway Relative to Four Global Atmospheric Reanalyses, Geophys Res Lett, 46, 6138–6147, https://doi.org/10.1029/2019GL082781, 2019.

Hack, J. J., Caron, J. M., Danabasoglu, G., Oleson, K. W., Bitz, C., and Truesdale, J. E.: CCSM-CAM3 Climate Simulation Sensitivity to Changes in Horizontal Resolution, 2006.

Hassler, B. and Lauer, A.: Comparison of reanalysis and observational precipitation datasets including era5 and wfde5, Atmosphere (Basel), 12, https://doi.org/10.3390/atmos12111462, 2021.

Hersbach, H., Bell, B., Berrisford, P., Hirahara, S., Horányi, A., Muñoz-Sabater, J., Nicolas, J., Peubey, C., Radu, R., Schepers, D., Simmons, A., Soci, C., Abdalla, S., Abellan, X., Balsamo, G., Bechtold, P., Biavati, G., Bidlot, J., Bonavita, M., De Chiara, G., Dahlgren, P., Dee, D., Diamantakis, M., Dragani, R., Flemming, J., Forbes, R., Fuentes, M., Geer, A., Haimberger, L., Healy, S., Hogan, R. J., Hólm, E., Janisková, M., Keeley, S., Laloyaux, P., Lopez, P., Lupu, C., Radnoti, G., de Rosnay, P., Rozum, I., Vamborg, F., Villaume, S., and Thépaut, J. N.: The ERA5 global reanalysis, Quarterly Journal of the Royal Meteorological Society, 146, 1999–2049, https://doi.org/10.1002/qj.3803, 2020.

Hersbach, H., Bell, B., Berrisford, P., Biavati, G., Horányi, A., Muñoz Sabater, J., Nicolas, J., Peubey, C., Radu, R., Rozum, I., Schepers, D., Simmons, A., Soci, C., Dee, D., Thépaut, J-N.: ERA5 hourly data on single levels from 1940 to present. Copernicus Climate Change Service (C3S) Climate Data Store (CDS), DOI: 10.24381/cds.adbb2d47, 2023 (Accessed on 16-09-2022).

Hertwig, E., von Storch, J. S., Handorf, D., Dethloff, K., Fast, I., and Krismer, T.: Effect of horizontal resolution on ECHAM6-AMIP performance, Clim Dyn, 45, 185–211, https://doi.org/10.1007/s00382-014-2396-x, 2015.

Hyndman, R. J. and Fan, Y.: Sample Quantiles in Statistical Packages, Source: The American Statistician, 361–365 pp., 1996.

Iles, C. E., Vautard, R., Strachan, J., Joussaume, S., Eggen, B. R., and Hewitt, C. D.: The benefits of increasing resolution in global and regional climate simulations for European climate extremes, Geosci Model Dev, 13, 5583–5607, https://doi.org/10.5194/gmd-13-5583-2020, 2020.

Intergovernmental Panel on Climate Change: Weather and Climate Extreme Events in a Changing Climate, in: Climate Change 2021 – The Physical Science Basis, Cambridge University Press, 1513–1766, https://doi.org/10.1017/9781009157896.013, 2023.

Jones, P. W.: First-and Second-Order Conservative Remapping Schemes for Grids in Spherical Coordinates, 1998.

Jong, B. T., Delworth, T. L., Cooke, W. F., Tseng, K. C., and Murakami, H.: Increases in extreme precipitation over the Northeast United States using high-resolution climate model simulations, NPJ Clim Atmos Sci, 6, https://doi.org/10.1038/s41612-023-00347-w, 2023.

Jung, T., Miller, M. J., Palmer, T. N., Towers, P., Wedi, N., Achuthavarier, D., Adams, J. M., Altshuler, E. L., Cash, B. A., Kinter, J. L., Marx, L., Stan, C., and Hodges, K. I.: High-resolution global climate simulations with the ECMWF model in project athena: Experimental design, model climate, and seasonal forecast skill, J Clim, 25, 3155–3172, https://doi.org/10.1175/JCLI-D-11-00265.1, 2012.

Khairoutdinov, M. and Kogan, Y.: A New Cloud Physics Parameterization in a Large-Eddy Simulation Model of Marine Stratocumulus, 2000.

Kopparla, P., Fischer, E. M., Hannay, C., and Knutti, R.: Improved simulation of extreme precipitation in a high-resolution atmosphere model, Geophys Res Lett, 40, 5803–5808, https://doi.org/10.1002/2013GL057866, 2013.

Kritsikis, E., Aechtner, M., Meurdesoif, Y., and Dubos, T.: Conservative interpolation between general spherical meshes, Geosci Model Dev, 10, 425–431, https://doi.org/10.5194/gmd-10-425-2017, 2017.

Lavers, D. A., Simmons, A., Vamborg, F., and Rodwell, M. J.: An evaluation of ERA5 precipitation for climate monitoring, Quarterly Journal of the Royal Meteorological Society, 148, 3152–3165, https://doi.org/10.1002/qj.4351, 2022.

Li, C., Zwiers, F., Zhang, X., Li, G., Sun, Y., and Wehner, M.: Changes in Annual Extremes of Daily Temperature and Precipitation in CMIP6 Models, J Clim, 34, 3441–3460, https://doi.org/10.1175/JCLI-D-19, 2021.

Li, F., Collins, W. D., Wehner, M. F., Williamson, D. L., Olson, J. G., and Algieri, C.: Impact of horizontal resolution on simulation of precipitation extremes in an aqua-planet version of Community Atmospheric Model (CAM3), n.d.

Malardel, S., Wedi, N., Deconinck, W., and Kühnlein, C.: A new grid for the IFS, 2016.

Manganello, J. V., Hodges, K. I., Kinter, J. L., Cash, B. A., Marx, L., Jung, T., Achuthavarier, D., Adams, J. M., Altshuler, E. L., Huang, B., Jin, E. K., Stan, C., Towers, P., and Wedi, N.: Tropical cyclone climatology in a 10-km global atmospheric GCM: Toward weather-resolving climate modeling, J Clim, 25, 3867–3893, https://doi.org/10.1175/JCLI-D-11-00346.1, 2012.

Masunaga, H., Schröder, M., Furuzawa, F. A., Kummerow, C., Rustemeier, E., and Schneider, U.: Inter-product biases in global precipitation extremes, Environmental Research Letters, 14, https://doi.org/10.1088/1748-9326/ab5da9, 2019.

Mishra, S. K. and Sahany, S.: Effects of time step size on the simulation of tropical climate in NCAR-CAM3, Clim Dyn, 37, 689–704, https://doi.org/10.1007/s00382-011-0994-4, 2011.

Monerie, P. A., Chevuturi, A., Cook, P., Klingaman, N. P., and Holloway, C. E.: Role of atmospheric horizontal resolution in simulating tropical and subtropical South American precipitation in HadGEM3-GC31, Geosci Model Dev, 13, 4749–4771, https://doi.org/10.5194/gmd-13-4749-2020, 2020.

Myhre, G., Alterskjær, K., Stjern, C. W., Hodnebrog, Marelle, L., Samset, B. H., Sillmann, J., Schaller, N., Fischer, E., Schulz, M., and Stohl, A.: Frequency of extreme precipitation increases extensively with event rareness under global warming, Sci Rep, 9, https://doi.org/10.1038/s41598-019-52277-4, 2019.

O'Gorman, P. A.: Precipitation Extremes Under Climate Change, https://doi.org/10.1007/s40641-015-0009-3, 1 June 2015.

Prein, A. F., Gobiet, A., Suklitsch, M., Truhetz, H., Awan, N. K., Keuler, K., and Georgievski, G.: Added value of convection permitting seasonal simulations, Clim Dyn, 41, 2655–2677, https://doi.org/10.1007/s00382-013-1744-6, 2013.

Roberts, C. D., Senan, R., Molteni, F., Boussetta, S., Mayer, M., and Keeley, S. P. E.: Climate model configurations of the ecmwf integrated forecasting system (ecmwf-ifs cycle 43r1) for highresmip, Geosci Model Dev, 11, 3681–3712, https://doi.org/10.5194/gmd-11-3681-2018, 2018.

Savita, A., Kjellsson, J., Kedzierski, R. P., Latif, M., Rahm, T., Wahl, S., and Park, W.: Assessment of climate biases in OpenIFS version 43r3 across model horizontal resolutions and time steps, Geosci Model Dev, 17, 1813–1829, https://doi.org/10.5194/gmd-17-1813-2024, 2024.

Schiemann, R., Demory, M. E., Mizielinski, M. S., Roberts, M. J., Shaffrey, L. C., Strachan, J., and Vidale, P. L.: The sensitivity of the tropical circulation and Maritime Continent precipitation to climate model resolution, Clim Dyn, 42, 2455–2468, https://doi.org/10.1007/s00382-013-1997-0, 2014.

Sillmann, J., Kharin, V. V., Zhang, X., Zwiers, F. W., and Bronaugh, D.: Climate extremes indices in the CMIP5 multimodel ensemble: Part 1. Model evaluation in the present climate, Journal of Geophysical Research Atmospheres, 118, 1716–1733, https://doi.org/10.1002/jgrd.50203, 2013.

Strandberg, G. and Lind, P.: The importance of horizontal model resolution on simulated precipitation in Europe – from global to regional models, Weather and Climate Dynamics, 2, 181–204, https://doi.org/10.5194/wcd-2-181-2021, 2021.

Sundqvist, H.: A parameterization scheme for non-convective condensation including prediction of cloud water content, Quarterly Journal of the Royal Meteorological Society, 104, 677–690, https://doi.org/10.1002/qj.49710444110, 1978.

Tarek, M., Brissette, F. P., and Arsenault, R.: Evaluation of the ERA5 reanalysis as a potential reference dataset for hydrological modelling over North America, Hydrol Earth Syst Sci, 24, 2527–2544, https://doi.org/10.5194/hess-24-2527-2020, 2020.

Tetzner, D., Thomas, E., and Allen, C.: A validation of ERA5 reanalysis data in the southern antarctic peninsula—Ellsworth land region, and its implications for ice core studies, Geosciences (Switzerland), 9, https://doi.org/10.3390/geosciences9070289, 2019.

Torma, C., Giorgi, F., and Coppola, E.: Added value of regional climate modeling over areas characterized by complex terrain-precipitation over the Alps, J Geophys Res, 120, 3957–3972, https://doi.org/10.1002/2014JD022781, 2015.

Wang, C., Graham, R. M., Wang, K., Gerland, S., and Granskog, M. A.: Comparison of ERA5 and ERA-Interim near-surface air temperature, snowfall and precipitation over Arctic sea ice: effects on sea ice thermodynamics and evolution, Cryosphere, 13, 1661–1679, https://doi.org/10.5194/tc-13-1661-2019, 2019.

Wehner, M. F., Smith, R. L., Bala, G., and Duffy, P.: The effect of horizontal resolution on simulation of very extreme US precipitation events in a global atmosphere model, Clim Dyn, 34, 241–247, https://doi.org/10.1007/s00382-009-0656-y, 2010.

Wehner, M. F., Reed, K. A., Li, F., Prabhat, Bacmeister, J., Chen, C. T., Paciorek, C., Gleckler, P. J., Sperber, K. R., Collins, W. D., Gettelman, A., and Jablonowski, C.: The effect of horizontal resolution on simulation quality in the Community Atmospheric Model, CAM5.1, J Adv Model Earth Syst, 6, 980–997, https://doi.org/10.1002/2013MS000276, 2014.

Xu, X., Frey, S. K., Boluwade, A., Erler, A. R., Khader, O., Lapen, D. R., and Sudicky, E.: Evaluation of variability among different precipitation products in the Northern Great Plains, J Hydrol Reg Stud, 24, https://doi.org/10.1016/j.ejrh.2019.100608, 2019.

Zhu, L. and Quiring, S. M.: Exposure to precipitation from tropical cyclones has increased over the continental United States from 1948 to 2019, Commun Earth Environ, 3, https://doi.org/10.1038/s43247-022-00639-8, 2022.

Ziese, Markus; Rauthe-Schöch, Armin; Becker, Andreas; Finger, Peter; Rustemeier, Elke; Hänsel, Stephanie; Schneider, Udo: GPCC Full Data Daily Version 2022 at 1.0°: Daily Land-Surface Precipitation from Rain-Gauges built on GTS-based and Historic Data. DOI: 10.5676/DWD_GPCC/FD_D_V2022_100, 2022
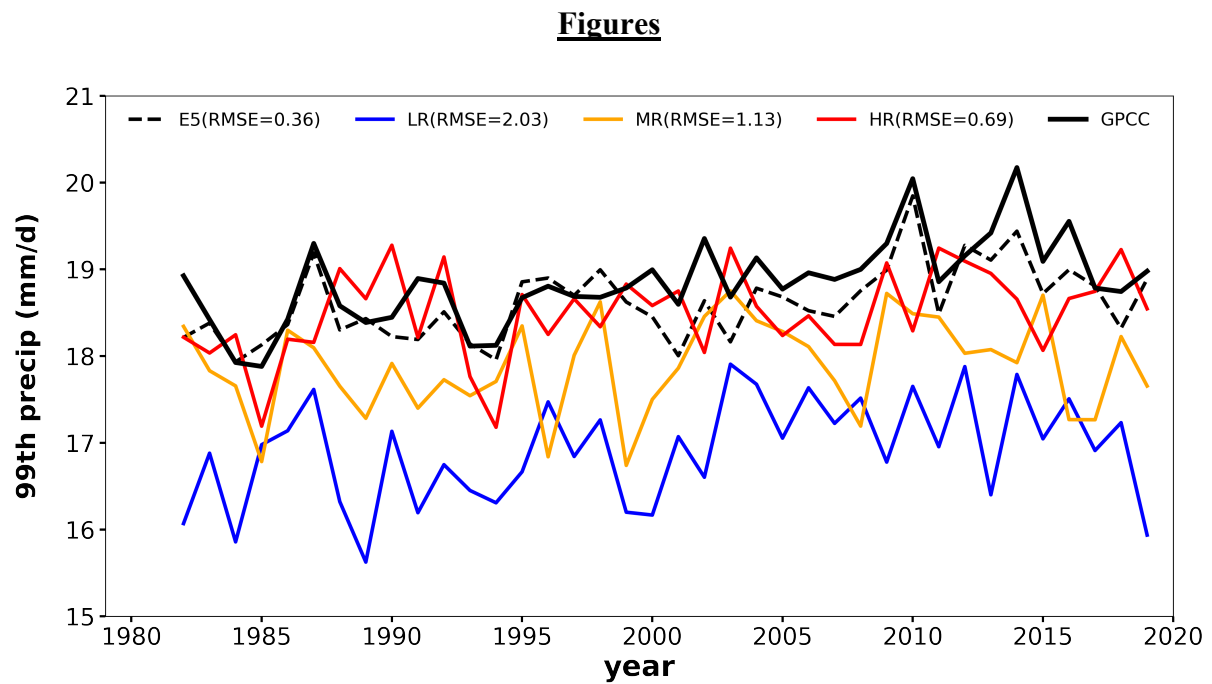
Figures

728
729

730   **Fig. 1** Annual time series of the 99th percentile precipitation using observations (GPCC, black

731   solid line), reanalysis (ERA5, black dash line), and model simulations (LR: blue, MR: orange,

732   HR: red) during 1982-2019 over Europe. RMSE values of 99th percentile precipitation are

733   computed referenced to GPCC which are shown within the small bracket (unit: mm/d).
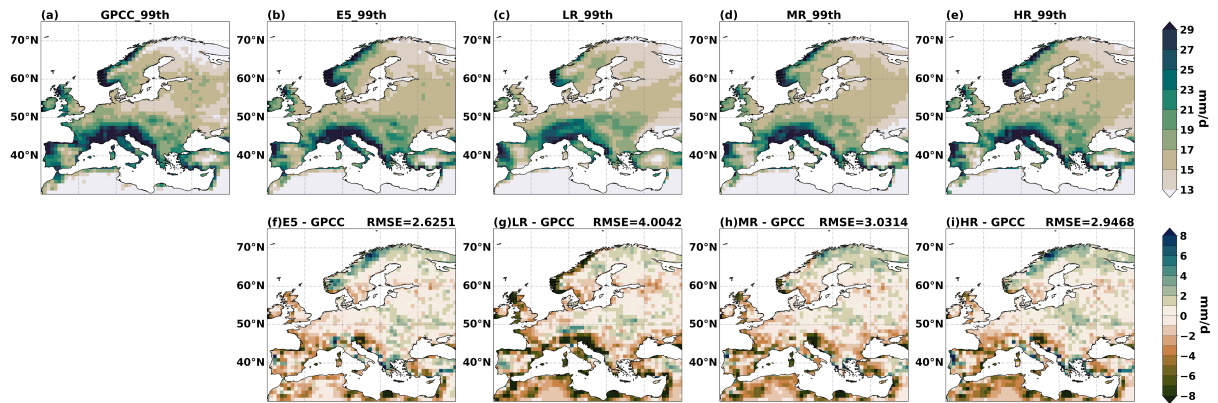
734
735
736
737
738
739
740
741
742
743
744
745
746
747
748
749
750
751
752
753
754
755

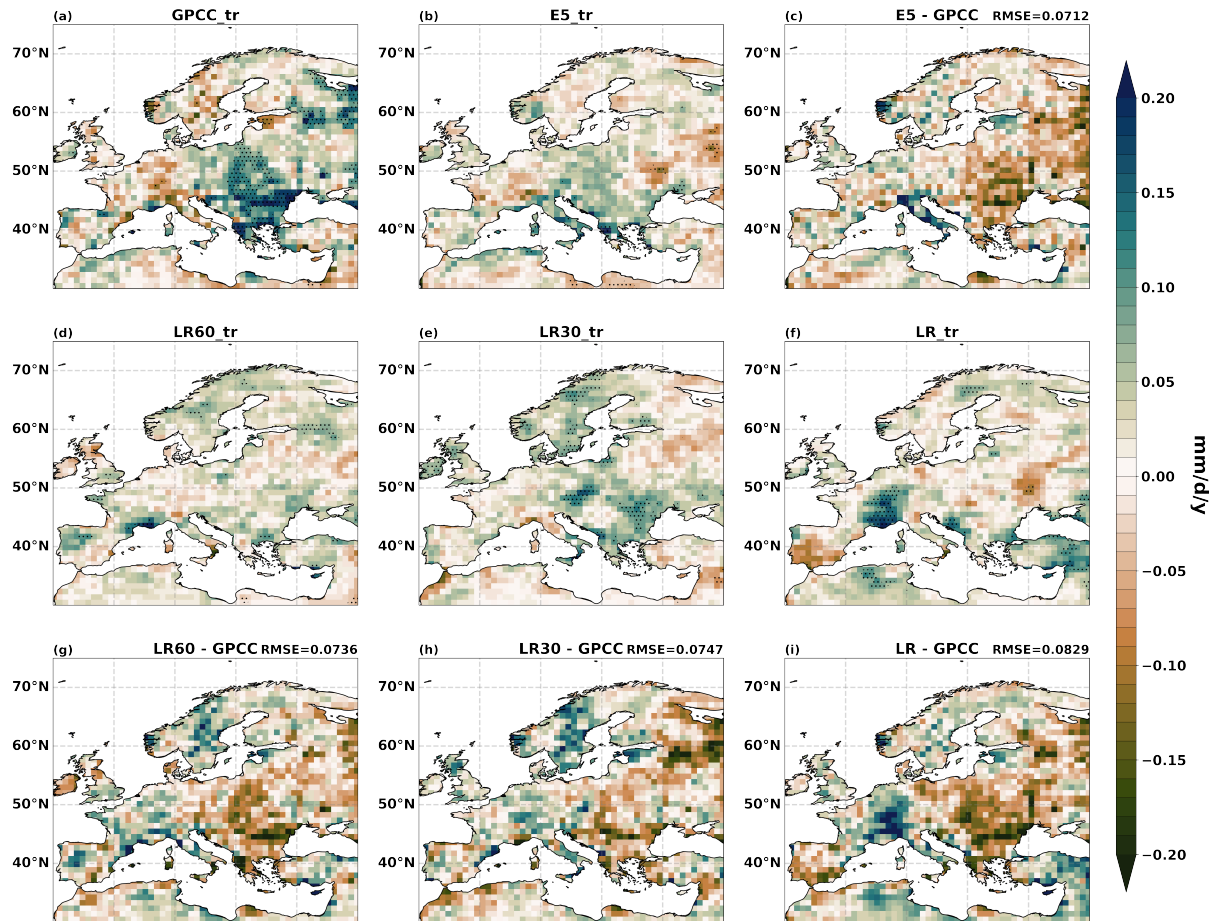**Fig. 2** The 99th percentile precipitation over Europe during 1982-2019 from (a) GPCC observations, (b) ERA5 reanalysis, (c) LR, (d) MR, (e) HR, and the corresponding biases and RMSEs in (f) ERA5, (g) LR, (h) MR, and (i) HR.

764
765
766
767
768
769
770
771
772
773
774
775
776
777
778
779
780
781
782
783
784
785
786
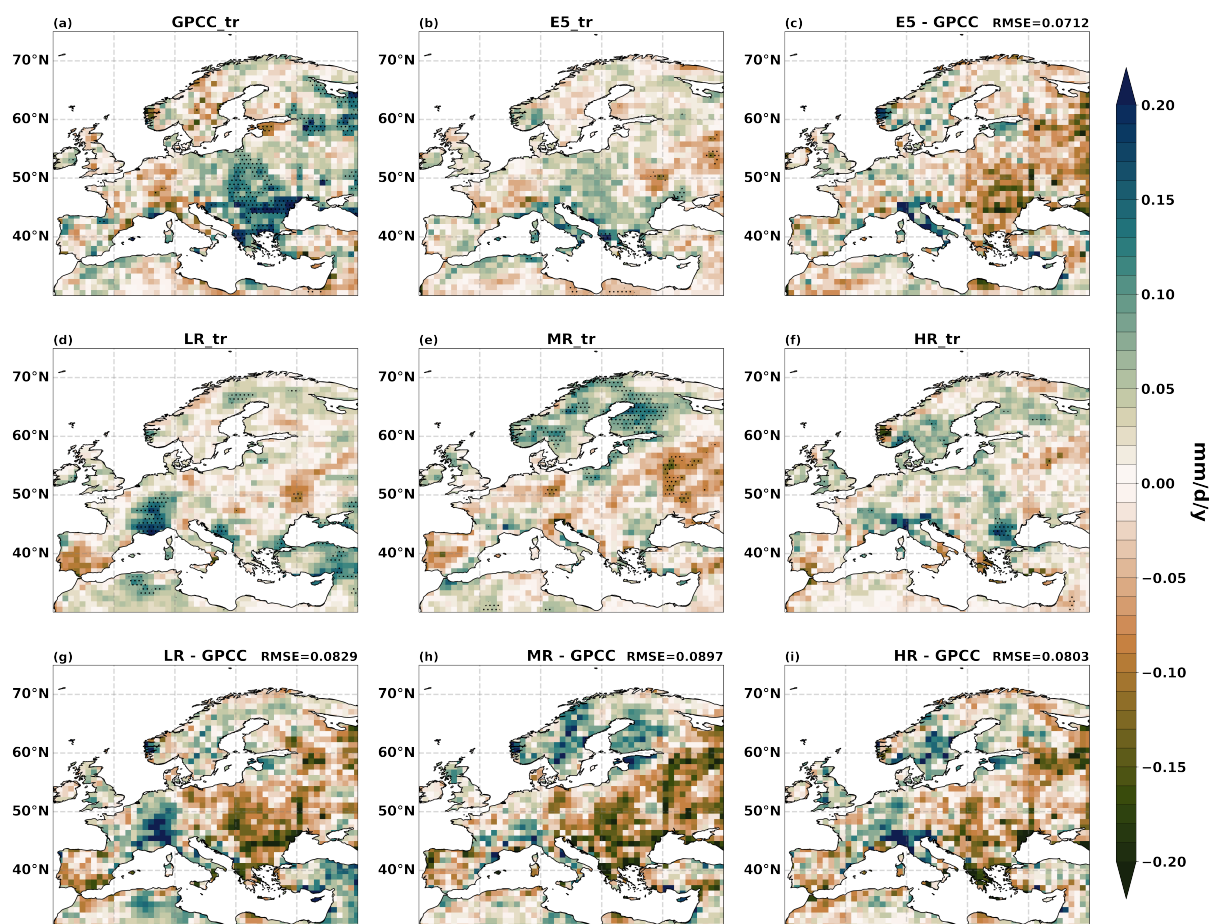
Fig. 3 The linear trends of annual 99th percentile precipitation over Europe during 1982-2019 from (a) GPCC observations, (b) ERA5 reanalysis, (d) LR, (e) MR, (f) HR, and the corresponding biases and RMSEs in (c) ERA5, (g) LR, (h) MR, (i) HR. The shadings are trends at 95 % significance levels.
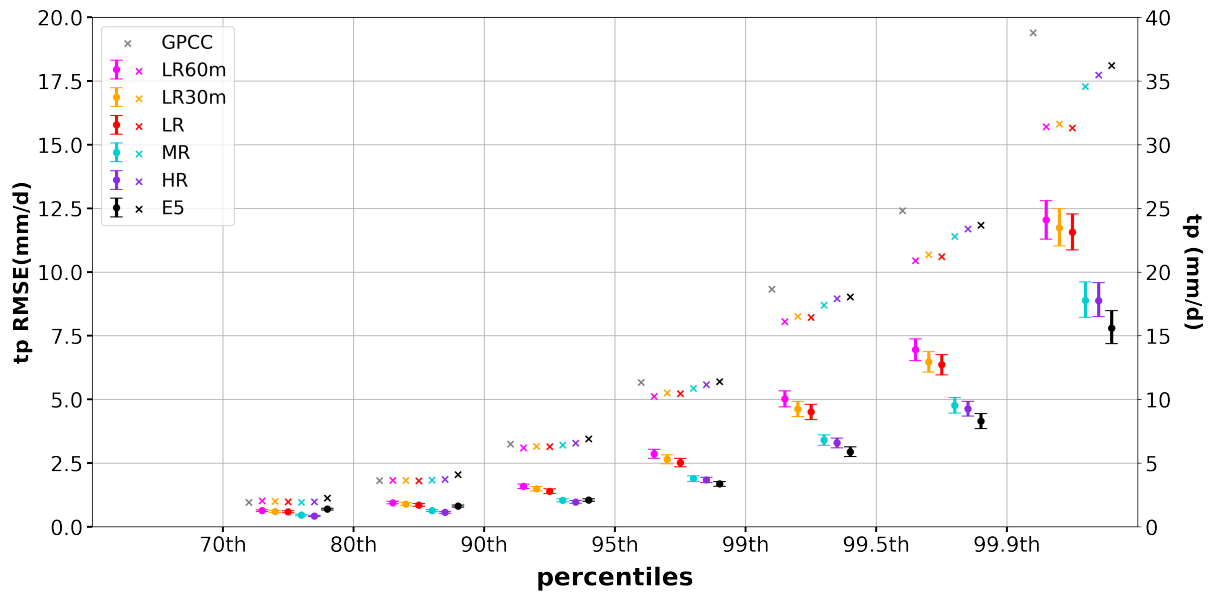
794 Fig. 4 The linear trends of annual 99th percentile precipitation over Europe during 1982-2019

795 from (a) GPCC observations, (b) ERA5 reanalysis, (d) LR60m, (e) LR30m, (f) LR, and the

796 corresponding biases and RMSEs in (c) ERA5, (g) LR60m, (h) LR30m, (i) LR. The shadings

797 are trends at 95 % significance levels.

Fig. 5 European averaged precipitation amounts and RMSEs (referenced to GPCC) for European total precipitation at different percentile ranges (70th – 80th, 80th – 90th, 90th – 95th, 95th – 99th, 99th – 99.5th, 99.5th – 99.9th and >99.9th percentile) in ERA5 (black) and OpenIFS simulations (LR60m: magenta, LR30m: orange, LR: red, MR: blue, HR: purple) during 1982-2019. Cross marks are the precipitation amounts. Dots are the RMSE values, and error bars are the 95 % CI.
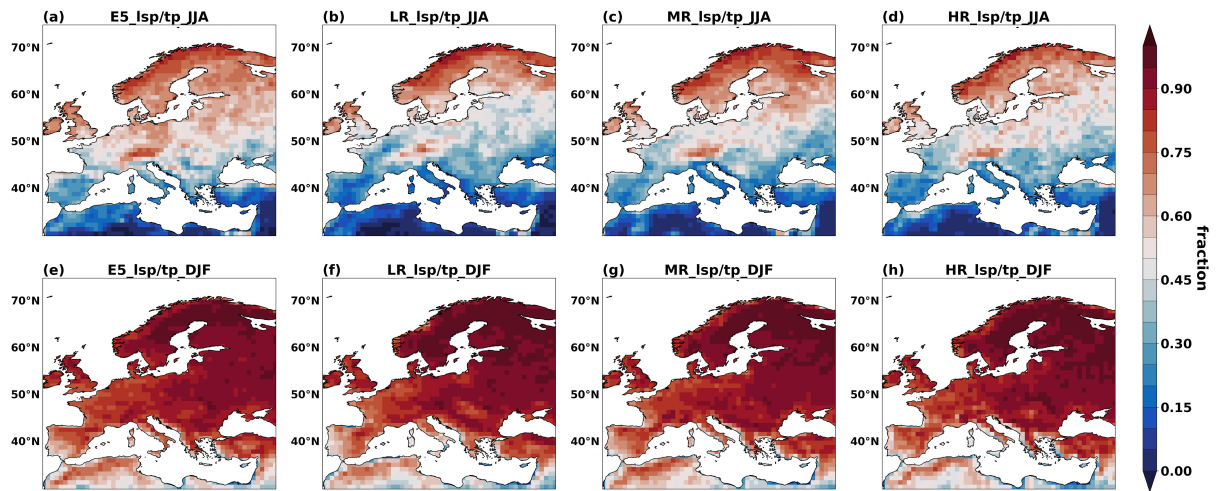
831

832 Fig. 6 Contribution of large-scale precipitation to extreme precipitation (>99th percentile) in

833 ERA5 (a & e), LR (b & f), MR (c & g) and HR (d & h) over Europe in JJA (a-d) and DJF (e-

834 h) over the period 1982-2019.

835

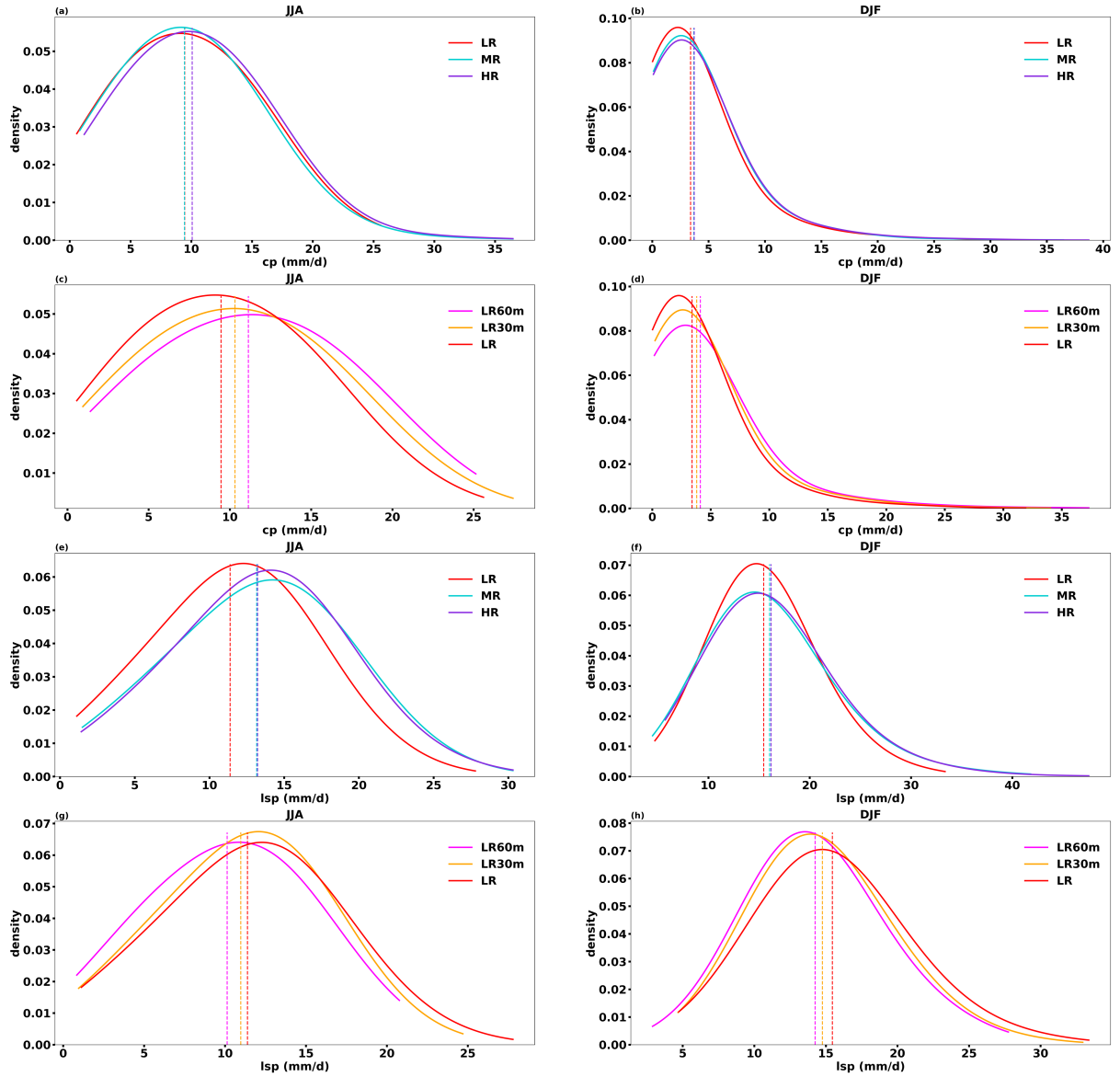836

837

838

839

840

841

842

843

844

845

846

847

Fig. 7 European convective (a-d) and large-scale precipitation (e-h) distribution across different horizontal resolutions (a, b, e and f) and model time steps (c, d, g and h) during extreme precipitation days in JJA and DJF (LR60m: magenta, LR30m: orange, LR: red, MR: blue, HR: purple). The time period is 1982-2019. The dash lines are the mean values of each distribution.
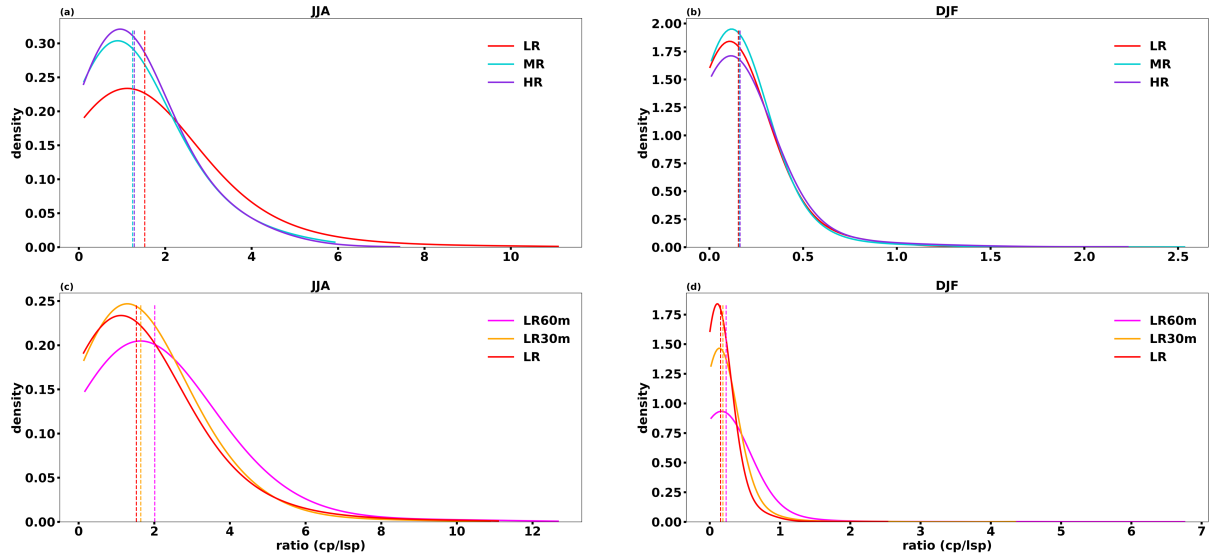
Fig. 8 The ratio between European convective and large-scale precipitation during extreme precipitation days across different horizontal resolutions (a & b) and model time steps (c & d) in JJA and DJF (LR60m: magenta, LR30m: orange, LR: red, MR: blue, HR: purple). The dash lines are the mean values of each distribution.
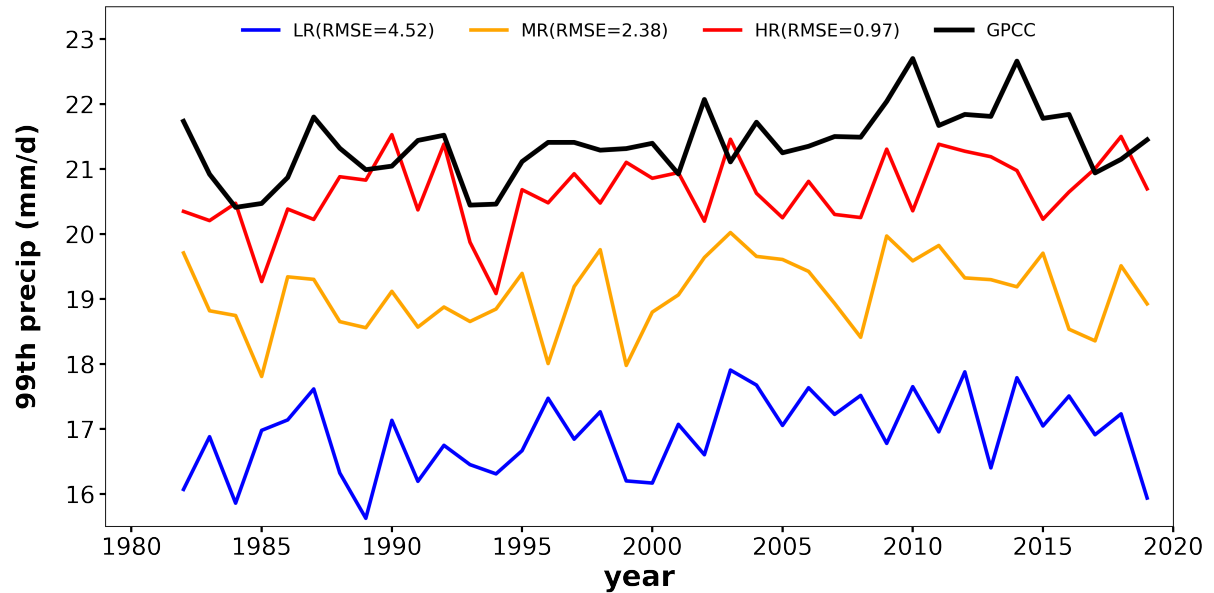

Fig. 9 Annual time series of the 99th percentile precipitation using observations (GPCC, black solid line) and model simulations on their native resolution (LR: blue, MR: orange, HR: red) during 1982-2019 over Europe. RMSE values of 99th percentile precipitation are computed referenced to GPCC which are shown within the small bracket (unit: mm/d).
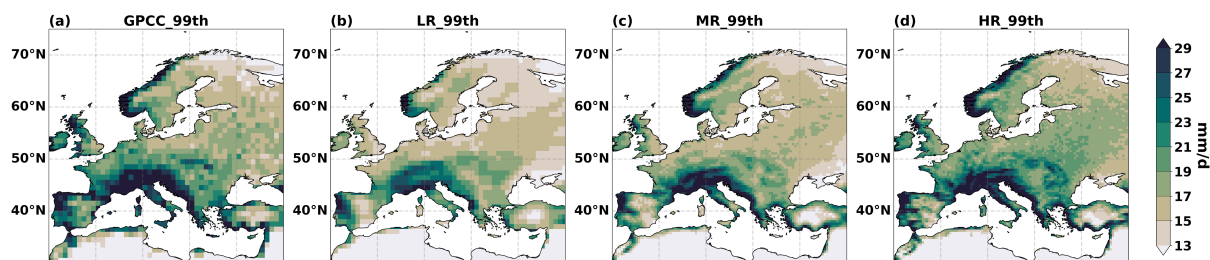
Fig. 10 The 99th percentile precipitation over Europe during 1982-2019 from (a) GPCC observations, (b) LR, (c) MR, (d) HR on their native resolution.
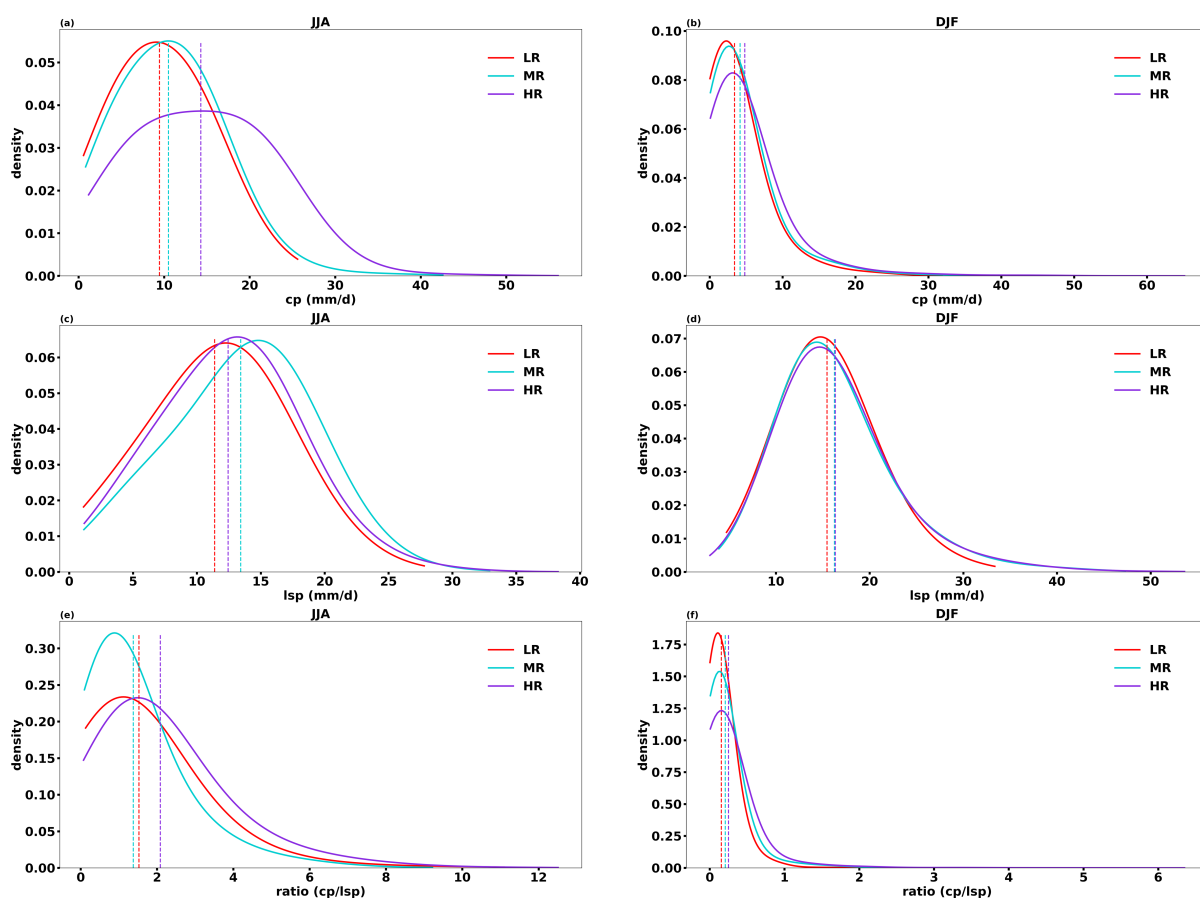

Fig. 11 European convective (a & b), large-scale precipitation (c & d) distribution and ratio (cp/lsp) on their native resolution across different horizontal resolutions during extreme precipitation days in JJA and DJF (LR: red, MR: blue, HR: purple). The time period is 1982-2019. The dash lines are the mean values of each distribution.

888
889
890   **Table**
891 Table 1: The experiment details of different horizontal resolutions and model time steps in
892 OpenIFS.

	LR60m	LR30m	LR	MR	HR
Vertical resolution	L91			L91	L91
Horizontal Resolution	100 km (Tco95)			50 km (Tco199)	25 km (Tco399)
Native output resolution	192×384			400×800	800×1600 (400×800 is used in the evaluation)
Regridded resolution	192×384			192×384	192×384
Time steps	60 minutes	30 minutes	15 minutes	15 minutes	15 minutes

893
894
895
896
897
898
899
900
901
902
903
904
905
906
907
908
909

Table 2: The p-values of t-test for convective (Table 2a), large-scale precipitation (Table 2b) and their ratios (Table 2c) distribution across horizontal resolutions and model time steps. The bold means significant (p-value < 0.05).

Table 2a

cp	JJA	DJF
LR → MR	0.92	**0.02**
MR → HR	**2.1 e-4**	0.75
LR60m → LR30m	**4.3 e-6**	**0.02**
LR30m → LR	**5.1 e-7**	**0.001**

Table 2b

lsp	JJA	DJF
LR → MR	**1.8 e-29**	**2.2 e-4**
MR → HR	0.70	0.39
LR60m → LR30m	**3.3 e-9**	**9.4 e-5**
LR30m → LR	**0.005**	**3.0 e-7**

Table 2c

ratio	JJA	DJF
LR → MR	**3.0 e-8**	0.49
MR → HR	0.37	0.64
LR60m → LR30m	**1.6 e-10**	**9.0 e-4**
LR30m → LR	**0.03**	**2.0 e-4**